NANO LETTERS

pubs.acs.org/NanoLett Letter

Gate-Tunable Anomalous Hall Effect in Stacked van der Waals Ferromagnetic Insulator–Topological Insulator Heterostructures

Andres E. Llacsahuanga Allcca,* Xing-Chen Pan, Ireneusz Miotkowski, Katsumi Tanigaki, and Yong P. Chen*

Cite This: *Nano Lett.* 2022, 22, 8130–8136 Read Online

ACCESS | Metrics & More | Article Recommendations | Supporting Information

ABSTRACT: The search of novel topological states, such as the quantum anomalous Hall insulator and chiral Majorana fermions, has motivated different schemes to introduce magnetism into topological insulators. A promising scheme is using the magnetic proximity effect (MPE), where a ferromagnetic insulator magnetizes the topological insulator. Most of these heterostructures are synthesized by growth techniques which prevent mixing many of the available ferromagnetic and topological insulators due to difference in growth conditions. Here, we demonstrate that MPE can be obtained in heterostructures stacked via the dry transfer of flakes of van der Waals ferromagnetic and topological insulators ($Cr_2Ge_2Te_6$/$BiSbTeSe_2$), as evidenced in the observation of an anomalous Hall effect (AHE). Furthermore, devices made from these heterostructures allow modulation of the AHE when controlling the carrier density via electrostatic gating. These results show that simple mechanical transfer of magnetic van der Waals materials provides another possible avenue to magnetize topological insulators by MPE.

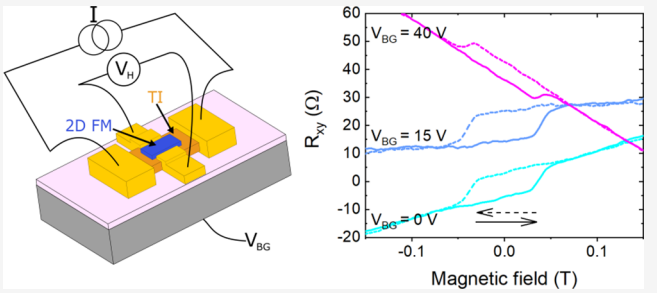

KEYWORDS: *magnetic proximity effect, topological insulator, 2D ferromagnetic insulators, van der Waals heterostructures, anomalous Hall effect*

In the attempts for the realization of new magnetic topological states, extrinsic (doping,[1] interfacing[2−6]) and intrinsic (magnetic topological insulators[7] or correlated Chern insulators in twisted bilayer graphene[8−11]) methods of integrating magnetism have been employed. Among them, it can be considered that engineering the interface holds the promise to be a more versatile platform for exploration; for example, the magnetic material and topological insulator can be chosen from a wide inventory of materials to create the heterostructures. The main limitation on interface engineering depends on the method to create the interface, for example, growing the materials on top of each other requires being mindful of lattice mismatch and chemical diffusion. Previously, this has been explored using metal–organic chemical vapor deposition (e.g., $Cr_2Ge_2Te_6$/Bi_2Te_3[4]) and molecular beam epitaxy (MBE) (e.g., EuS/Bi_2Se_3,[12] $Y_3Fe_5O_{12}$/Bi_2Se_3,[13] $Y_3Fe_5O_{12}$/$(Bi_xSb_{1-x})_2Te_3$,[14] $Tm_3Fe_5O_{12}$/$(Bi_xSb_{1-x})_2Te_3$,[15] $Eu_3Fe_5O_{12}$/$(Bi,Sb)_2Te_3$,[16] $Cr_2Ge_2Te_6$/$(Bi_xSb_{1-x})_2Te_3$,[2,3,17] and (Zn,Cr)Te/$(Bi,Sb)_2Te_3$/(Zn,Cr)Te[18]). More recently, wet transfer (e.g., $Y_3Fe_5O_{12}$/Bi_2Se_3,[19] $Cr_2Ge_2Te_6$/$BiSbTeSe_2$[6]) and dry transfer ($Cr_2Ge_2Te_6$/$BiSbTeSe_2$[5]) have also been used to assemble the heterostructures using layered or van der Waals (vdW) materials that can help relax the requirements such as lattice matching for interface engineering. In principle, the weak interlayer coupling in vdW materials makes possible the use of simple mechanical transfer to create an interface free from the issues or limits in growth techniques. In this work, we prepare van der Waals heterostructures using such a mechanical dry transfer method. By choosing an appropriate bulk-insulating topological insulator (TI) along with an insulating van der Waals ferromagnet, we show that the heterostructures of these materials exhibit an anomalous Hall effect (AHE). Importantly and in contrast to previous similarly fabricated (wet and dry transfer) samples, our observed AHE shows clear hysteresis. Furthermore, due to the bulk-insulating nature of the chosen topological insulator, it is possible to change its carrier density by electrostatic gating. This is shown to be able to modulate the amplitude of the AHE (while its sign remains unchanged) following a similar trend to that of the longitudinal resistance of the device when tuning the back gate voltage. These results are interpreted as a magnetic proximity effect induced in the top surface states of the topological insulator due to the ferromagnetic insulator,

Received: June 29, 2022
Revised: October 5, 2022
Published: October 10, 2022

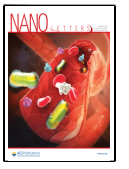

https://doi.org/10.1021/acs.nanolett.2c02571
Nano Lett. 2022, 22, 8130–8136

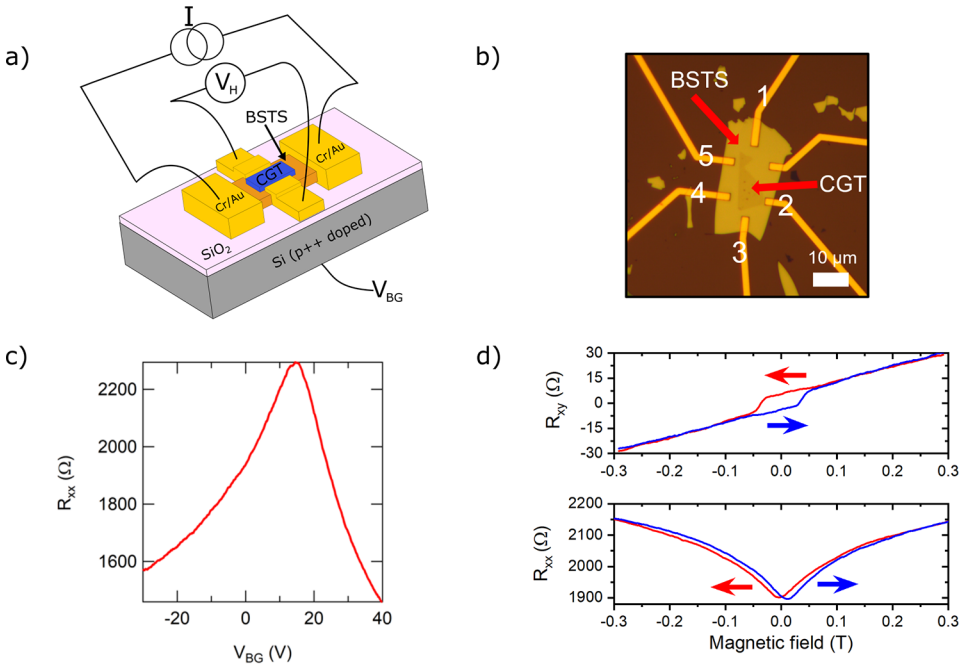

Figure 1. (a) Schematic of the $Cr_2Ge_2Te_6$/$BiSbTeSe_2$ (CGT/BSTS) back gated device (not showing all electrodes; only the ones injecting the current I and measuring the Hall voltage V_H are shown). (b) Optical microscope image of a device, numbers indicate the electrodes used to measure R_{xx} (5 to 4) and R_{xy} (2 to 4) and inject current (1 to 3) for the 4-terminal measurements. CGT thickness is 6 nm, and BSTS thickness is 66 nm. Scale bar is 10 μm. (c) Longitudinal resistance (R_{xx}) as a function of the back-gate voltage (V_{BG}) at T = 2 K and B = 0 T. Ambipolar field effect is observed. (d) Hall resistance ($R_{xy} = V_H/I$) and longitudinal resistance (R_{xx}) measured at ~2 K and V_{BG} = 0 V as functions of an out-of-plane magnetic field (B), showing clear hysteresis. Correspondingly colored arrows indicate magnetic field sweep directions.

realized in a fully vdW heterostructure bypassing growth constraints and limitations found in previous works. The gate tunability can be largely explained by a two-channel model involving a magnetized top surface with an AHE in parallel to a gate-tunable bottom surface. The ability to magnetize local/selective areas of the top surface of a topological insulator (something that can be more challenging in growth-based approaches) is also important in various proposed schemes to manipulate and measure Majorana fermions in superconductor/topological insulator hybrids.[20,21]

We use thin flakes mechanically exfoliated from the vdW layered $Cr_2Ge_2Te_6$ (CGT) as the ferromagnetic insulator in our heterostructure. Single crystals of this material were grown via a self-flux technique as described in a previous work.[22] For the topological insulator, we employ flakes exfoliated from a single crystal of $BiSbTeSe_2$ (BSTS) grown by the vertical Bridgman technique as described in ref 23. Taking advantage of the layered nature of these crystals, it is possible to assemble heterostructures while avoiding those defects and irregularities in the interface that might occur in heterostructures assembled via growth due to lattice mismatch and chemical diffusion (both issues can be detrimental for AHE observation).[2,24] We chose topological insulator flakes with a thickness in the range of 40−70 nm, which maintain the intrinsic insulating bulk and conduct mainly through the surface states.[23,25,26] For the ferromagnetic insulator, we chose flakes with a thickness in the range of 4−10 nm, whose low temperature magnetization shows a more rectangular hysteresis loop with a clear coercivity and higher remnant magnetization compared to the smooth magnetization behavior for bulk CGT and the more complicated hysteresis loops with softer magnetic behavior in thicker CGT flakes (>10 nm).[27] The latter are usually attributed to the formation of labyrinth type domains[28,29] (see Figure S1 for an evolution of hysteresis loops of CGT as thickness is increased, measured using Magneto Optics Kerr Effect). This distinct magnetic hysteresis loop behavior was expected to be inherited into the topological insulator and would make the AHE more distinguishable from other nonlinear Hall effects. In Figure 1a and b, a schematic of the heterostructures and the microscope image of a typical device are shown, respectively. As can be seen, the CGT flake did not fully cover the topological insulator. This was done to ease the contact fabrication, as CGT is highly insulating at low temperatures (see Figure S2) and a full coverage of the BSTS flakes would lead to poor contacts. In Figure 1c, an ambipolar field effect in the longitudinal resistance measured by the four-probe method can be observed, showcasing that the heterostructure still allows similar gate tuning of the resistance as in BSTS-only devices.[23] An out-of-plane magnetic field is applied and swept to extract the Hall resistance in the samples. Figure 1d shows representative traces of the Hall resistance and longitudinal resistance vs magnetic field for the device. As seen in the figure, a clear AHE with a rectangular hysteresis loop with an amplitude of a few ohms and a coercive field of ~0.035 T is observed in the R_{xy} curve, indicating that a magnetization in the conducting carriers is introduced by interfacing the topological insulator BSTS with the magnetic insulator CGT. Furthermore, the longitudinal resistance (R_{xx}) of the device shows a minimum in the magnetoresistance around zero field, typically attributed to the weak antilocalization (WAL) behavior due to the strong spin orbit coupling in the topological insulator. Phenomenologically, the magnetoresistance can be fitted to the Hikami−Larkin−Nagaoka equation used to describe the WAL, and how the fitting parameters vary with the back gate (see Figure S3) is similar to the WAL behavior reported in the literature.[30,31]

https://doi.org/10.1021/acs.nanolett.2c02571
Nano Lett. 2022, 22, 8130−8136

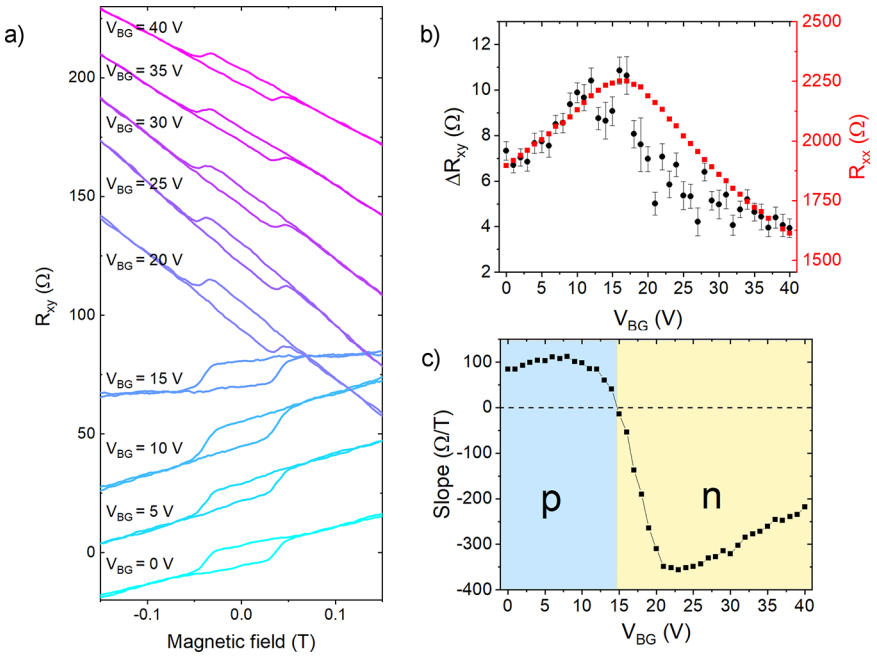

Figure 2. (a) Magnetic field dependent hall resistance (R_{xy}) measured for different back-gate voltages (V_{BG}) for the device shown in Figure 1. Two traces labeled by their V_{BG} correspond to opposite magnetic field sweeps (the trace with higher/lower R_{xy} at the hysteresis loop is measured with decreasing/increasing magnetic field). All measurements done at T = 2 K with an excitation DC current of 10 μA. Traces are offset for clarity. (b) Amplitude of the resistance hysteresis due to anomalous Hall effect, ΔR_{xy} (obtained after subtracting a polynomial background in magnetic field dependent R_{xy} data, see Supplemental Figure S5 for an example), plotted on the left axis as a function of V_{BG}. The R_{xx} data (right axis) were extracted from the average of the R_{xx} minima in the two traces with opposite magnetic field sweeps (such as those in Figure 1d lower panel). (c) Slope (related to the ordinary Hall effect) of the linear part of the background in the R_{xy} vs magnetic field, plotted as a function of V_{BG}. The sign change indicates a change in the dominant type of carriers.

To further study the hysteresis loop (attributed to AHE) in R_{xy}, the main focus of this paper, we measure R_{xy} as the function of the gate voltage (V_{BG}, applied to the silicon substrate as a global back gate), shown in Figure 2a. As can be seen, there is a change in the magnitude of the hysteresis loop along with a changing slope of the linear background in the Hall resistance for changing V_{BG}. After removing a smooth polynomial background, the step size ΔR_{xy} (assigned as the amplitude of AHE) of the hysteresis loop can be obtained. The result is plotted as a function of the V_{BG} in Figure 2b, showing a tunability in the AHE amplitude from ∼4 Ω to ∼11 Ω. The longitudinal resistance R_{xx} (measured at the minimum of the magnetoresistance) is also plotted as a function of V_{BG} in the same figure, and a correlation with ΔR_{xy} is observed. The extracted Hall coefficient (linear slope of R_{xy} vs magnetic field, reflecting the ordinary Hall effect) is plotted in Figure 2c and is clearly modulated (both the sign and amplitude) by the back gate. The change in the sign indicates the tunability of the dominant carrier type in the device from holes to electrons (note the discussions generally hold even in the case that our BSTS flakes consist of two independent surface channels, with the bottom channel tuned more by the back gate, to be discussed in more detail later). The amplitude of the Hall coefficient achieved in both carrier regimes would correspond to a carrier concentration on the order of few 10^{12} cm^{-2}, similar to previous BSTS devices in the literature.[26,5,23,33]

The fact that the hysteresis loop maintains its direction, or that the AHE (ΔR_{xy}) does not change its sign, even when the Hall coefficient changes the sign or dominant carrier type is changed is a significant observation, as it rules out the trivial Hall effect due to any stray magnetic field produced by the ferromagnet (CGT) as a possible cause for the R_{xy} hysteresis (in the trivial Hall effect scenario the hysteresis or ΔR_{xy} would also change sign when the main carrier type or Hall slope changes sign).[14,32] Furthermore, we have estimated that the strength of the fringe magnetic field in such devices (no more than 1 mT[27,34]) is too weak to produce the observed ΔR_{xy} (of ∼10 Ω, which would require a change in magnetic field on the order 0.1 T, as seen in Figure 1d).

We also studied the temperature dependence of the AHE. Figure 3a shows the evolution of R_{xy} as the temperature is increased, where the hysteresis loop (AHE amplitude ΔR_{xy},

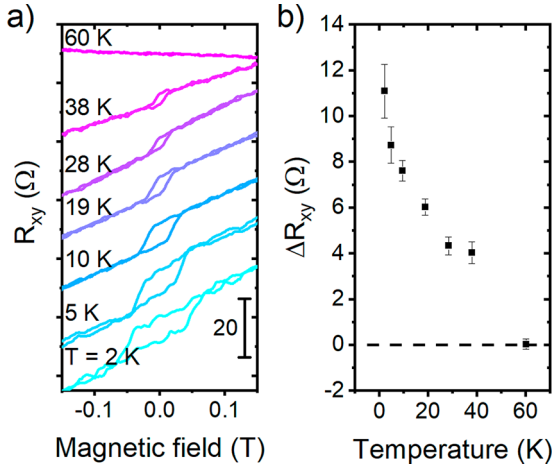

Figure 3. (a) Hall resistance (R_{xy} vs magnetic field) for different temperatures (traces offset for clarity) and (b) hysteresis amplitude related to the anomalous Hall effect (right, ΔR_{xy}) as a function of temperature. Dashed line marks the zero level.

https://doi.org/10.1021/acs.nanolett.2c02571
Nano Lett. 2022, 22, 8130−8136

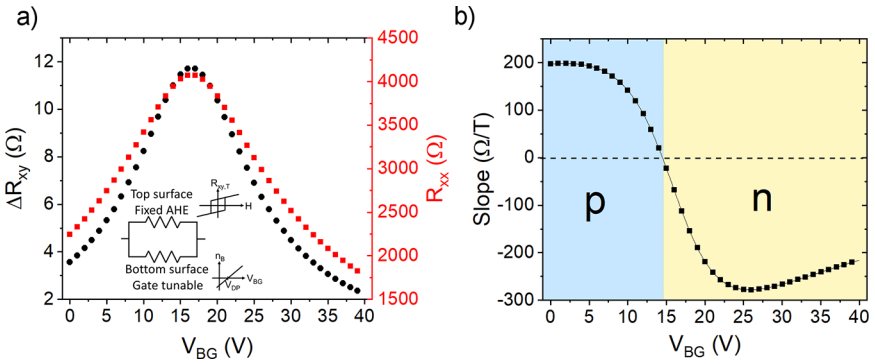

Figure 4. Gate-tuned resistance and AHE in a two-channel model. (a) The calculated amplitude of the AHE (left axis) and total R_{xx} (right axis) due to two parallel conduction channels consisting of a top surface with fixed anomalous Hall effect and fixed resistance and a bottom surface with gate tunable resistance (as shown in the inset), as functions of V_{BG}. (b) Slope of the linear part of the background in the calculated total R_{xy} vs magnetic field, plotted as a function of V_{BG}. The parameters used for these results are detailed in the Supporting Information.

Figure 3b) is seen to vanish between 38 and 60 K. This is consistent with the Curie temperature ($T_C \sim 50$ K) of CGT flakes of comparable thickness measured with the magneto-optics Kerr effect in previous work.[22] In Figures S4 and S5, we further show the temperature dependence of the AHE in additional devices along with magneto optics Kerr effect (MOKE) hysteresis loops measured at the same time, showcasing that the AHE behavior measured by the magneto transport is consistent with the CGT magnetization probed by MOKE. The temperature dependence of the longitudinal resistance R_{xx} is shown in Figure S6. The observed metallic behavior is consistent with our previous measurement of similar BSTS flakes (whose conduction is dominated by the metallic surface state at such temperatures).[23] It is worth noting that our BSTS flake is only partially covered by CGT on the top surface; therefore the unmagnetized bottom surface and unmagnetized portion of the top surface are expected to make an important contribution to R_{xx}.

Finally, to further shed light onto the gate tunability of the AHE, we present a simple model of two parallel channels of conduction that can largely reproduce key features of our results (the details are left to the Supporting Information). The model consists of two conduction channels representing a gate tunable bottom surface without AHE and a top surface with fixed AHE (not gate-tunable, motivated by the experimental situation that the top surface is much less affected by the electrostatic gating in BSTS with a similar thickness to that which we used[33]). Figure 4a and b show the AHE amplitude, R_{xx}, and slope of R_{xy} as a function of gate voltage calculated using our simple model. The results indicate that a fixed channel with AHE can give rise to similar gate tunability to what we experimentally observe when connected in parallel with a gate-tunable channel with no AHE, and the change of AHE amplitude for the device can be explained based on the resistance change of the bottom surface that is gated.

Our measurement in CGT shows that it becomes highly insulating with negligible conductance at low temperatures (Figure S2). While the AHE could in principle also arise from CGT that becomes conductive after charge transfer from BSTS, we believe this is a less likely scenario to explain our observations. Previous studies on TI/CGT have noted moderate hole doping in the TI due to charge (hole) transfer from CGT (equivalently, electron transfer from TI to CGT).[3,6] Our own measurements, also suggest a similar moderate hole doping in BSTS (no more than $\sim 10^{12}$ cm^{-2}) based on the shift of the charge neutral point toward a positive gate voltage in our transport measurements in comparison to our earlier measurements done on BSTS-only, where the charge neutral point occurs at negative voltages.[23] However, our measurements on CGT-only (Figure S2, exhibiting a weak field effect of p-type behavior) as well as prior measurements on CGT (e.g., refs 35, 36) all showed that the CGT is p-doped itself. Therefore, for the expected hole doping in BSTS after interfacing with CGT (therefore n-doping or electron transfer on CGT), the charge transfer would make CGT more intrinsic and even more insulating (as indeed shown in previous field-effect studies in CGT such as[35]) thus unlikely to become a conducting channel exhibiting its own AHE. Finally, a very large charge transfer from our TI to CGT to make it conductive would heavily dope the TI, and this is not consistent with the actual observed field effects in our devices.

In conclusion, we demonstrated that thin flakes of the topological insulator BSTS can show an anomalous Hall effect when interfaced with thin flakes of CGT using simple mechanical dry transfer methods for the assembly. The observed AHE shows a rectangular hysteresis loop with a coercive field of ~0.035 T at 2 K and vanishes close to the T_C of thin CGT flakes. Furthermore, the AHE can be tuned from ~4 to ~11 Ω and follows the longitudinal resistance of the device as a back gate is applied. These results indicate that simple mechanical transfer of van der Waals materials allows for a magnetic proximity effect in the surface state of a topological insulator, a basis to realize novel magnetic topological phases such as QAHI and to implement various proposed devices schemes for measuring and manipulating Majorana fermions in topological insulator/superconductor hybrid structures. Our work may further facilitate interfacing the growing inventory of layered materials with different magnetic or electrical properties.

EXPERIMENTAL METHODS

Device Fabrication. BSTS and CGT thin flakes were exfoliated on SiO_2/Si substrates inside a glovebox, where the oxygen and water concentration were less than 5 ppm. We chose appropriate CGT thin flakes (thickness between 4−10 nm) and BSTS flakes (thickness between 40−70 nm) based on the optical contrast with the thickness later confirmed by atomic force microscopy. We transferred the freshly exfoliated CGT flakes using the dry transfer technique on top of fresh BSTS flakes. Briefly, we used a PDMS/polycarbonate (PC)

https://doi.org/10.1021/acs.nanolett.2c02571
Nano Lett. 2022, 22, 8130−8136

stamp to transfer the CGT flake from its initial substrate to the top of the chosen BSTS flake, the CGT flake is dropped along with the PC carrier film. To remove the PC film the sample is rinsed with chloroform for 10 min followed by acetone and isopropyl alcohol solvent cleaning. Then, the heterostructure is patterned using electron beam lithography. Finally, 5 nm of Cr and 95 nm of Au are deposited as contacts using e-beam evaporation. The prepared devices are then mounted for electrical transport measurements as quickly as possible after liftoff, usually with no more than half an hour to an hour of exposure to air to avoid degradation of CGT.

Electrical Transport Measurements. Electrical transport measurements are performed in a variable temperature insert (VTI) system, which allows temperatures from 1.8 K to 300 K and an applied magnetic field of up to 6 T. The longitudinal resistance and Hall resistance were measured using a four probe method with a Stanford Research SR830 lock-in amplifier with a low frequency (∼13 Hz) excitation current of 100 nA to 1 μA or by applying 1−10 μA of DC current with a Keithley 2400 source meter and measuring the voltage drop with a Keithley 2182A nanovoltmeter. The gate control was achieved by applying a DC voltage to the p-doped silicon substrate using a Keithley 2400 source meter. The magnetic field-dependent Hall resistance traces were antisymmetrized between traces measured with decreasing and increasing magnetic field (i.e., $R_{xy\ \mathrm{antisym}}(B) = (R_{xy\ \mathrm{B\ decreasing}}(B) - R_{xy\ \mathrm{B\ increasing}}(-B))/2$). This is done to remove some field-even features from the Hall effect traces resulting from the mixing of R_{xx} into the R_{xy} due to the geometry of the device and misalignment of electrodes. It is worth noting that the hysteresis loops and AHE modulation with a back gate are still evident without the antisymmetrization step.

■ ASSOCIATED CONTENT

Supporting Information

The Supporting Information is available free of charge at https://pubs.acs.org/doi/10.1021/acs.nanolett.2c02571.

Thickness dependence of the hysteresis loops of the magnetization of CGT (as probed with MOKE, Figure S1), temperature dependence of current in bare CGT indicating its insulating nature at low temperatures (Figure S2), the HLN equation fits to the magneto-resistance (Figure S3), AHE in other devices and their temperature dependence (Figure S4), comparison of MOKE and AHE measured on the same CGT/TI device (Figure S5), and the temperature dependence of R_{xx} (Figure S6); a description of the simple model used for Figure 4a and b detailed along with the parameters used (PDF)

■ AUTHOR INFORMATION

Corresponding Authors

Andres E. Llacsahuanga Allcca − *Department of Physics and Astronomy, Purdue University, West Lafayette, Indiana 47907, United States; Purdue Quantum Science and Engineering Institute and Birck Nanotechnology Center, Purdue University, West Lafayette, Indiana 47907, United States;* orcid.org/0000-0003-0414-5613; Email: aallcca@purdue.edu

Yong P. Chen − *Department of Physics and Astronomy and School of Electrical and Computer Engineering, Purdue University, West Lafayette, Indiana 47907, United States; Purdue Quantum Science and Engineering Institute and Birck Nanotechnology Center, Purdue University, West Lafayette, Indiana 47907, United States; WPI Advanced Institute for Materials Research (AIMR) and Center for Science and Innovation in Spintronics, Tohoku University, Sendai 980-8577, Japan; Institute of Physics and Astronomy and Villum Center for Hybrid Quantum Materials and Devices, Aarhus University, 8000 Aarhus-C, Denmark*; Email: yongchen@purdue.edu

Authors

Xing-Chen Pan − *WPI Advanced Institute for Materials Research (AIMR), Tohoku University, Sendai 980-8577, Japan*

Ireneusz Miotkowski − *Department of Physics and Astronomy, Purdue University, West Lafayette, Indiana 47907, United States*

Katsumi Tanigaki − *WPI Advanced Institute for Materials Research (AIMR), Tohoku University, Sendai 980-8577, Japan; Beijing Academy of Quantum Information Sciences, Beijing 100193, China*

Complete contact information is available at: https://pubs.acs.org/10.1021/acs.nanolett.2c02571

Notes

The authors declare no competing financial interest.

■ ACKNOWLEDGMENTS

We acknowledge P. Upadhyaya, J. Liao, G. Cheng, and J. Ribeiro for fruitful discussions. Different stages of this research at Purdue have been supported in part by National Science Foundation Emerging Frontiers & Multidisciplinary Activities (EFMA #1641101) and the U.S. Department of Energy (DOE) Office of Science through the Quantum Science Center (QSC, a National Quantum Information Science Research Center). Work at Tohoku has been supported in part by JSPS KAKENHI (Grants No. 17K14329, No. 18H04471, No. 18H04304, No. 18F18328, and No. 18H03858) and the thermal management program of CREST, JST, research grants from The Iwatani Naoji Foundation's Research Grant, and AIMR with the support of World Premier International Research Center Initiative (WPI) from MEXT. X.-C.P. acknowledges the support from an International Research Fellowship of Japan Society for the Promotion of Science [Postdoctoral Fellowships for Research in Japan (Standard)]. K.T. acknowledges the support from the National Natural Science Foundation of China (Grant No. 12174027).

■ REFERENCES

(1) Chang, C.-Z.; Zhang, J.; Feng, X.; Shen, J.; Zhang, Z.; Guo, M.; Li, K.; Ou, Y.; Wei, P.; Wang, L.-L.; Ji, Z.-Q.; Feng, Y.; Ji, S.; Chen, X.; Jia, J.; Dai, X.; Fang, Z.; Zhang, S.-C.; He, K.; Wang, Y.; Lu, L.; Ma, X.-C.; Xue, Q.-K. Experimental Observation of the Quantum Anomalous Hall Effect in a Magnetic Topological Insulator. *Science* **2013**, *340* (6129), 167−170.

(2) Yao, X.; Gao, B.; Han, M.; Jain, D.; Moon, J.; Kim, J. W.; Zhu, Y.; Cheong, S.; Oh, S. Record High-Proximity-Induced Anomalous Hall Effect in $(Bi_xSb_{1-x})_2Te_3$ Thin Film Grown on $CrGeTe_3$ Substrate. *Nano Lett.* **2019**, *19* (7), 4567−4573.

(3) Mogi, M.; Nakajima, T.; Ukleev, V.; Tsukazaki, A.; Yoshimi, R.; Kawamura, M.; Takahashi, K. S.; Hanashima, T.; Kakurai, K.; Arima, T.; Kawasaki, M.; Tokura, Y. Large Anomalous Hall Effect in

Topological Insulators with Proximitized Ferromagnetic Insulators. *Phys. Rev. Lett.* **2019**, *123* (1), 016804.
(4) Alegria, L. D.; Ji, H.; Yao, N.; Clarke, J. J.; Cava, R. J.; Petta, J. R. Large Anomalous Hall Effect in Ferromagnetic Insulator-Topological Insulator Heterostructures. *Appl. Phys. Lett.* **2014**, *105* (5), 053512.
(5) Chong, S. K.; Han, K. B.; Nagaoka, A.; Tsuchikawa, R.; Liu, R.; Liu, H.; Vardeny, Z. V.; Pesin, D. A.; Lee, C.; Sparks, T. D.; Deshpande, V. V. Topological Insulator-Based van Der Waals Heterostructures for Effective Control of Massless and Massive Dirac Fermions. *Nano Lett.* **2018**, *18* (12), 8047−8053.
(6) Nagata, K.; Matsushita, S. Y.; Pan, X.-C.; Huynh, K.-K.; Tanigaki, K. Large-Proximity-Induced Anomalous Hall Effect in $Bi_{2-x}Sb_xTe_{3-y}Se_y/Cr_2Ge_2Te_6$ heterostructure prepared by film transfer method. *Phys. Rev. Mater.* **2021**, *5* (2), 024208.
(7) Liu, C.; Wang, Y.; Li, H.; Wu, Y.; Li, Y.; Li, J.; He, K.; Xu, Y.; Zhang, J.; Wang, Y. Robust Axion Insulator and Chern Insulator Phases in a Two-Dimensional Antiferromagnetic Topological Insulator. *Nat. Mater.* **2020**, *19* (5), 522−527.
(8) Sharpe, A. L.; Fox, E. J.; Barnard, A. W.; Finney, J.; Watanabe, K.; Taniguchi, T.; Kastner, M. A.; Goldhaber-Gordon, D. Emergent Ferromagnetism near Three-Quarters Filling in Twisted Bilayer Graphene. *Science* **2019**, *365* (6453), 605−608.
(9) Chen, G.; Sharpe, A. L.; Fox, E. J.; Zhang, Y. H.; Wang, S.; Jiang, L.; Lyu, B.; Li, H.; Watanabe, K.; Taniguchi, T.; Shi, Z.; Senthil, T.; Goldhaber-Gordon, D.; Zhang, Y.; Wang, F. Tunable Correlated Chern Insulator and Ferromagnetism in a Moiré Superlattice. *Nature* **2020**, *579* (7797), 56−61.
(10) Polshyn, H.; Zhu, J.; Kumar, M. A.; Zhang, Y.; Yang, F.; Tschirhart, C. L.; Serlin, M.; Watanabe, K.; Taniguchi, T.; MacDonald, A. H.; Young, A. F. Electrical Switching of Magnetic Order in an Orbital Chern Insulator. *Nature* **2020**, *588* (7836), 66−70.
(11) Stepanov, P.; Xie, M.; Taniguchi, T.; Watanabe, K.; Lu, X.; Macdonald, A. H.; Bernevig, B. A.; Efetov, D. K. Competing Zero-Field Chern Insulators in Superconducting Twisted Bilayer Graphene. *Phys. Rev. Lett.* **2021**, *127* (19), 197701.
(12) Wei, P.; Katmis, F.; Assaf, B. A.; Steinberg, H.; Jarillo-Herrero, P.; Heiman, D.; Moodera, J. S. Exchange-Coupling-Induced Symmetry Breaking in Topological Insulators. *Phys. Rev. Lett.* **2013**, *110* (18), 1−5.
(13) Lang, M.; Montazeri, M.; Onbasli, M. C.; Kou, X.; Fan, Y.; Upadhyaya, P.; Yao, K.; Liu, F.; Jiang, Y.; Jiang, W.; Wong, K. L.; Yu, G.; Tang, J.; Nie, T.; He, L.; Schwartz, R. N.; Wang, Y.; Ross, C. A.; Wang, K. L. Proximity Induced High-Temperature Magnetic Order in Topological Insulator - Ferrimagnetic Insulator Heterostructure. *Nano Lett.* **2014**, *14* (6), 3459−3465.
(14) Jiang, Z.; Chang, C.; Tang, C.; Wei, P.; Moodera, J. S.; Shi, J. Independent Tuning of Electronic Properties and Induced Ferromagnetism in Topological Insulators with Heterostructure Approach. *Nano Lett.* **2015**, *15* (9), 5835−5840.
(15) Tang, C.; Chang, C. Z.; Zhao, G.; Liu, Y.; Jiang, Z.; Liu, C. X.; McCartney, M. R.; Smith, D. J.; Chen, T.; Moodera, J. S.; Shi, J. Above 400-K Robust Perpendicular Ferromagnetic Phase in a Topological Insulator. *Sci. Adv.* **2017**, *3* (6), 2−7.
(16) Zou, W. J.; Guo, M. X.; Wong, J. F.; Huang, Z. P.; Chia, J. M.; Chen, W. N.; Wang, S. X.; Lin, K. Y.; Young, L. B.; Lin, Y. H. G.; Yahyavi, M.; Wu, C. T.; Jeng, H. T.; Lee, S. F.; Chang, T. R.; Hong, M.; Kwo, J. Enormous Berry-Curvature-Based Anomalous Hall Effect in Topological Insulator $(Bi,Sb)_2Te_3$ on Ferrimagnetic Europium Iron Garnet beyond 400 K. *ACS Nano* **2022**, *16* (2), 2369−2380.
(17) Mogi, M.; Yasuda, K.; Fujimura, R.; Yoshimi, R.; Ogawa, N.; Tsukazaki, A.; Kawamura, M.; Takahashi, K. S.; Kawasaki, M.; Tokura, Y. Current-Induced Switching of Proximity-Induced Ferromagnetic Surface States in a Topological Insulator. *Nat. Commun.* **2021**, *12* (1), 3−8.
(18) Watanabe, R.; Yoshimi, R.; Kawamura, M.; Mogi, M.; Tsukazaki, A.; Yu, X. Z.; Nakajima, K.; Takahashi, K. S.; Kawasaki, M.; Tokura, Y. Quantum Anomalous Hall Effect Driven by Magnetic Proximity Coupling in All-Telluride Based Heterostructure. *Appl. Phys. Lett.* **2019**, *115* (10), 102403.
(19) Che, X.; Murata, K.; Pan, L.; He, Q. L.; Yu, G.; Shao, Q.; Yin, G.; Deng, P.; Fan, Y.; Ma, B.; Liang, X.; Zhang, B.; Han, X.; Bi, L.; Yang, Q. H.; Zhang, H.; Wang, K. L. Proximity-Induced Magnetic Order in a Transferred Topological Insulator Thin Film on a Magnetic Insulator. *ACS Nano* **2018**, *12* (5), 5042−5050.
(20) Hasan, M. Z.; Kane, C. L. Colloquium: Topological Insulators. *Rev. Mod. Phys.* **2010**, *82* (4), 3045−3067.
(21) Papaj, M.; Fu, L. Creating Majorana Modes from Segmented Fermi Surface. *Nat. Commun.* **2021**, *12* (1), 1−7.
(22) Idzuchi, H.; Llacsahuanga Allcca, A. E.; Pan, X. C.; Tanigaki, K.; Chen, Y. P. Increased Curie Temperature and Enhanced Perpendicular Magneto Anisotropy of $Cr_2Ge_2Te_6$/NiO Heterostructures. *Appl. Phys. Lett.* **2019**, *115* (23), 232403.
(23) Xu, Y.; Miotkowski, I.; Liu, C.; Tian, J.; Nam, H.; Alidoust, N.; Hu, J.; Shih, C.-K.; Hasan, M. Z.; Chen, Y. P. Observation of Topological Surface State Quantum Hall Effect in an Intrinsic Three-Dimensional Topological Insulator. *Nat. Phys.* **2014**, *10* (12), 956−963.
(24) Bhattacharyya, S.; Akhgar, G.; Gebert, M.; Karel, J.; Edmonds, M. T.; Fuhrer, M. S. Recent Progress in Proximity Coupling of Magnetism to Topological Insulators. *Adv. Mater.* **2021**, *33* (33), 1−30.
(25) Xu, Y.; Jiang, G.; Miotkowski, I.; Biswas, R. R.; Chen, Y. P. Tuning Insulator-Semimetal Transitions in 3D Topological Insulator Thin Films by Intersurface Hybridization and In-Plane Magnetic Fields. *Phys. Rev. Lett.* **2019**, *123* (20), 207701.
(26) Chong, S. K.; Han, K. B.; Sparks, T. D.; Deshpande, V. V. Tunable Coupling between Surface States of a Three-Dimensional Topological Insulator in the Quantum Hall Regime. *Phys. Rev. Lett.* **2019**, *123* (3), 36804.
(27) Noah, A.; Alpern, H.; Singh, S.; Gutfreund, A.; Zisman, G.; Feld, T. D.; Vakahi, A.; Remennik, S.; Paltiel, Y.; Huber, M. E.; Barrena, V.; Suderow, H.; Steinberg, H.; Millo, O.; Anahory, Y. Interior and Edge Magnetization in Thin Exfoliated $CrGeTe_3$ Films. *Nano Lett.* **2022**, *22* (7), 3165−3172.
(28) Jagla, E. A. Hysteresis Loops of Magnetic Thin Films with Perpendicular Anisotropy. *Phys. Rev. B* **2005**, *72* (9), 094406.
(29) Fei, Z.; Huang, B.; Malinowski, P.; Wang, W.; Song, T.; Sanchez, J.; Yao, W.; Xiao, D.; Zhu, X.; May, A. F.; Wu, W.; Cobden, D. H.; Chu, J.-H.; Xu, X. Two-Dimensional Itinerant Ferromagnetism in Atomically Thin Fe_3GeTe_2. *Nat. Mater.* **2018**, *17* (9), 778−782.
(30) Steinberg, H.; Laloë, J.-B.; Fatemi, V.; Moodera, J. S.; Jarillo-Herrero, P. Electrically Tunable Surface-to-Bulk Coherent Coupling in Topological Insulator Thin Films. *Phys. Rev. B* **2011**, *84* (23), 233101.
(31) Jauregui, L. A.; Pettes, M. T.; Rokhinson, L. P.; Shi, L.; Chen, Y. P. Gate Tunable Relativistic Mass and Berry's Phase in Topological Insulator Nanoribbon Field Effect Devices. *Sci. Rep.* **2015**, *5* (1), 8452.
(32) Wang, Z.; Tang, C.; Sachs, R.; Barlas, Y.; Shi, J. Proximity-Induced Ferromagnetism in Graphene Revealed by the Anomalous Hall Effect. *Phys. Rev. Lett.* **2015**, *114* (1), 016603.
(33) Fatemi, V.; Hunt, B.; Steinberg, H.; Eltinge, S. L.; Mahmood, F.; Butch, N. P.; Watanabe, K.; Taniguchi, T.; Gedik, N.; Ashoori, R. C.; Jarillo-Herrero, P. Electrostatic Coupling between Two Surfaces of a Topological Insulator Nanodevice. *Phys. Rev. Lett.* **2014**, *113* (20), 1−5.
(34) Kim, M.; Kumaravadivel, P.; Birkbeck, J.; Kuang, W.; Xu, S. G.; Hopkinson, D. G.; Knolle, J.; McClarty, P. A.; Berdyugin, A. I.; Ben Shalom, M.; Gorbachev, R. V.; Haigh, S. J.; Liu, S.; Edgar, J. H.; Novoselov, K. S.; Grigorieva, I. V.; Geim, A. K. Micromagnetometry of Two-Dimensional Ferromagnets. *Nat. Electron.* **2019**, *2* (10), 457−463.
(35) Xing, W.; Chen, Y.; Odenthal, P. M.; Zhang, X.; Yuan, W.; Su, T.; Song, Q.; Wang, T.; Zhong, J.; Jia, S.; Xie, X. C.; Li, Y.; Han, W. Electric Field Effect in Multilayer $Cr_2Ge_2Te_6$: A Ferromagnetic 2D Material. *2D Mater.* **2017**, *4* (2), 024009.

https://doi.org/10.1021/acs.nanolett.2c02571
Nano Lett. 2022, 22, 8130−8136

(36) Wang, Z.; Zhang, T.; Ding, M.; Dong, B.; Li, Y.; Chen, M.; Li, X.; Huang, J.; Wang, H.; Zhao, X.; Li, Y.; Li, D.; Jia, C.-K.; Sun, L.; Guo, H.; Ye, Y.; Sun, D.-M.; Chen, Y.-S.; Yang, T.; Zhang, J.; Ono, S.; Han, Z.; Zhang, Z.-D. Electric-Field Control of Magnetism in a Few-Layered van Der Waals Ferromagnetic Semiconductor. *Nat. Nanotechnol.* **2018**, *13* (7), 554−559.

https://doi.org/10.1021/acs.nanolett.2c02571
Nano Lett. 2022, 22, 8130−8136